PCCP

PAPER

View Article Online
View Journal

Cite this: DOI: 10.1039/d6cp00604c

Fast and ultrafast charge transfer dynamics in organic dye sensitizers anchored on TiO_2 for photoelectrochemical cells

Federica Ruani, [a] Matteo Bartolini, [b] Elena Ermini, [bc] Elisa Bandini, [a] Andrea Barbieri, [a] Adalgisa Sinicropi, [bd] Alessandro Mordini, [bc] Lorenzo Zani *[b] and Barbara Ventura *[a]

Received 18th February 2026,
Accepted 14th April 2026

DOI: 10.1039/d6cp00604c

rsc.li/pccp

Three organic conjugated donor–acceptor dyes with hydrophobic side chains were studied as potential photosensitizers for dye-sensitized photoelectrochemical cells (DS-PECs). The dyes were anchored on TiO_2 electrodes and investigated using steady-state and femtosecond transient absorption spectroscopies. Optical studies revealed intramolecular charge transfer (ICT) as the dominant excitation pathway, with **AD418** showing single-state emission and **BTD-DTP1/TTZ5** displaying dual ICT emission. On TiO_2, ultrafast electron injection (1–2 ps) leads to long-lived mono-cationic species, indicating effective charge separation.

Introduction

Photoelectrochemical cell (PEC) technology has garnered significant attention as a promising avenue for efficient solar energy conversion, particularly for applications such as water splitting and the generation of chemical fuels.[1] PEC systems integrate light absorption and catalytic electrochemical reactions within a single device, enabling sunlight to be converted into a flow of electrons that directly drives endothermic chemical processes. By coupling photoactive materials with electrochemical interfaces, PEC cells mimic natural photosynthesis to efficiently harness solar irradiation for sustainable energy conversion, including the direct production of hydrogen fuel.[2] The design of tandem PEC cells, utilizing complementary photoactive materials in the photoanode and photocathode, has demonstrated the capacity to operate under neutral pH conditions with visible light, yielding advancements in efficiency and stability.[3] Such systems can achieve notable light-to-hydrogen conversion efficiencies, making them attractive for renewable fuel production.

In a PEC cell, semiconductor materials absorb sunlight to generate electron–hole pairs, which then drive the required redox reactions, such as water splitting into hydrogen and oxygen. However, many semiconductors with good electrochemical properties (such as TiO_2) have wide bandgaps and are only active under ultraviolet light, which constitutes a small portion of the solar spectrum. To address this limitation, dye-sensitized photoelectrochemical cells (DS-PECs) have been developed.[4,5] In these configurations, organic or metal–organic dyes that absorb visible light are anchored onto the surface of wide-bandgap semiconductors. These dyes act as light harvesters, capturing a broader range of the solar spectrum and transferring the excited electrons to the conduction band of the anodic semiconductor.[6] The electrons are then transferred to the counter-electrode (cathode), where they will be used to reduce water to hydrogen. Eventually, the process is completed with the dye regeneration by a suitable electron donor which, in the presence of an appropriate catalyst,[7] could be water itself (thus giving rise to full water splitting).[8]

Suitable dyes for DS-PEC applications need to possess certain unique characteristics, such as: (i) proper frontier energy level alignment to guarantee electron transfer towards the semiconductor, (ii) wide and intense light absorption in the visible region, (iii) strong anchoring to the semiconductor and (iv) adequate chemical and photochemical stability. There is a vast library of compounds that can act as sensitizers, such as ruthenium complexes, porphyrins bearing transition metals and full organic dyes but, among those, the latter offer some advantages, *i.e.*, the potential to efficiently gather visible light because of their high molar absorption coefficients and the chance to avoid the usage of costly and/or toxic metals.

[a] *Istituto per la Sintesi Organica e la Fotoreattività (ISOF), Consiglio Nazionale delle Ricerche (CNR), Via Gobetti 101, 40129 Bologna, BO, Italy. E-mail: barbara.ventura@cnr.it*
[b] *Istituto di Chimica dei Composti Organometallici (ICCOM), Consiglio Nazionale delle Ricerche (CNR), Via Madonna del Piano 10, 50019 Sesto Fiorentino, Italy. E-mail: lorenzo.zani@cnr.it*
[c] *Dipartimento di Chimica "U. Schiff", Università degli Studi di Firenze, Via della Lastruccia 13, 50019 Sesto Fiorentino, Italy*
[d] *Dipartimento di Biotecnologie, Chimica e Farmacia, Università di Siena, R^2ES Lab, Via Aldo Moro 2, 53100 Siena, Italy*

In recent years, donor–π–acceptor (D–π–A) organic dyes have emerged as a focal point of research in the development of DS-PECs, driven by their potential to enhance light absorption, improve charge separation, and boost overall cell efficiency. The design of these organic sensitizers is primarily concerned with optimizing their photophysical properties, such as molar absorption coefficients, spectral response, and charge transfer dynamics.[9] Their development has seen significant advancements, essentially driven by strategic molecular engineering.[10–12]

Indeed, optimizing solar energy conversion requires precise features at the molecular structure level, including the presence of tailored functional groups, highly conjugated π-bridges and appropriate donor–acceptor combinations. Extending π-bridges, for example with dithiophene units, enhances light harvesting and electron transfer by increasing donor–acceptor separation and reducing charge recombination.[13] Charge separation is further governed by the strength and nature of electron-donating groups and spacers, while strong acceptors, like diketopyrrolopyrrole and benzothiadiazole, broaden absorption and improve solar spectral overlap.[14–20] The use of anchoring groups alternative to carboxylic acids, such as pyridine- or phosphonic acid–based moieties, also improves device stability and photochemical performance.[21–23] Collectively, these molecular modifications have enabled state-of-the-art DS-PEC water-splitting devices to achieve photocurrent densities of several hundred μA cm^{-2},[17] with faradaic efficiencies exceeding 80%, underscoring the effectiveness of rational dye design.[24]

Emerging trends in dye design have also explored the stability and operational conditions of organic compounds in relevant environments. It has been demonstrated that the integration of new linkers and moieties improves interfacial electron transfer and the overall robustness of organic dyes under varied operational settings.[25] Furthermore, more complex molecular configurations, such as donor–π–acceptor–acceptor (D–π–2A) systems, have already been shown to facilitate effective electron transfer to semiconductor substrates.[26,27]

Recent advances in the understanding of charge transfer mechanisms have propelled PEC technology forward. Investigations into the dynamics of charge-separated states have highlighted the critical role of electron transfer between the dye and the semiconductor substrate.[28,29] Time-resolved laser spectroscopy provides a flexible and effective method for studying charge carrier dynamics, with transient absorption (TA) being one of the most powerful techniques for this kind of investigations.[30]

In the last few years, we synthesized three organic dyes incorporating different heterocyclic units, namely **AD418**,[31] **BTD-DTP1**,[32] and **TTZ5**[33] (Fig. 1), that provided promising results as photosensitizers for dye-sensitized solar cells (DSSC)[32–34] and dye-sensitized photocatalytic systems for H_2 production (DSP).[31] The three dyes share some common characteristics: (i) the presence of long hydrophobic side chains, that decrease the chance of dye deactivation or desorption from the semiconductor by preventing water from adhering to the TiO_2 surface, and suppress undesirable dye aggregation; (ii) a terminal triphenyl amine group as donor unit; (iii) a heterocyclic core based on N and S heteroatoms as spacer and (iv) a CN group as additional acceptor moiety.

In this work, we sought to gain a deeper understanding of the interfacial charge transfer processes involving the above-mentioned dyes after adsorption onto nanocrystalline TiO_2, aiming to evaluate their effectiveness in acting as photosensitizers for DS-PEC applications. Therefore, screen-printed TiO_2 photoelectrodes sensitized with the three dyes were systematically characterized using steady-state optical spectroscopy and femtosecond transient absorption measurements, to elucidate the excited-state deactivation pathways and charge carrier dynamics that govern the photosensitization performance.

Results and discussion

Synthesis

Dyes **AD418**, **BTD-DTP1** and **TTZ5** were synthesized according to the procedures reported in our previous works.[31,32,35] The

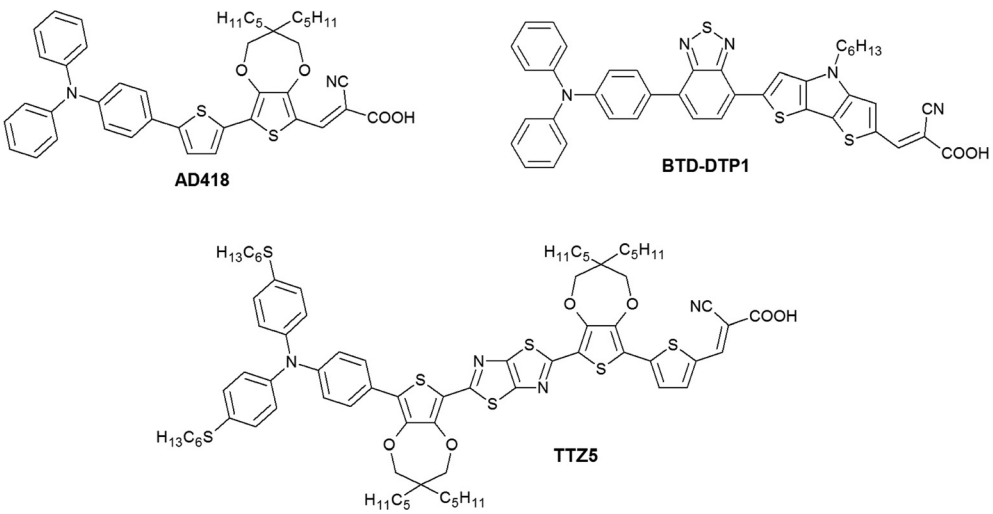

Fig. 1 Chemical structures of **AD418**, **BTD-DTP1**, and **TTZ5** dyes.

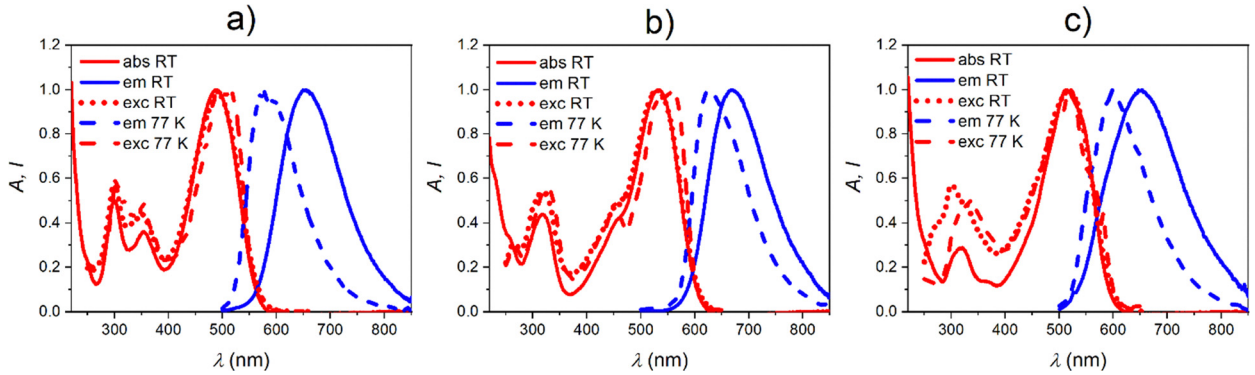

Fig. 2 Normalized UV-Vis absorption (red full lines), corrected emission (blue full lines, λ_{exc} = 455 nm) and excitation (red dotted lines, λ_{em} = 700 nm) spectra of **AD418** (a), **BTD-DTP1** (b), and **TTZ5** (c) in THF solution at r.t. Normalized excitation (red dashed lines) and emission (blue dashed lines) spectra in CH_2Cl_2 : MeOH (1 : 1) glassy mixture at 77 K.

Table 1 Main photophysical parameters of investigated dyes

	Absorption[a]	Emission at r.t.[a]			Emission at 77 K[b]	
	λ, nm (ε, M^{-1} cm^{-1})	λ, nm[c]	ϕ[d]	τ, ns[e]	λ, nm[c]	τ, ns[e]
AD418	485 (38 600)	653	0.469	2.5	574	2.5
BTD-DTP1	532 (64 300)	669	0.448	2.6 (80%)	626	1.9 (48%)
				4.7 (20%)		3.9 (52%)
TTZ5	513 (94 100)	652	0.115	0.9 (83%)	601	1.3 (78%)
				2.9 (17%)		2.6 (22%)

[a] In THF solution at room temperature. [b] In CH_2Cl_2 : CH_3OH (1 : 1) glassy mixture at 77 K. [c] From spectra corrected for the detector response. [d] With reference to $[Ru(bpy)_3]Cl_2$ in H_2O (ϕ = 0.042), λ_{exc} = 460 nm. [e] λ_{exc} = 465 nm.

corresponding schemes and a brief description of the synthetic routes are reported in the SI (Schemes S1–S3).

Photophysics

Absorption and emission spectroscopy. The absorption spectra of the dyes **AD418**, **BTD-DTP1**, and **TTZ5**, recorded in THF solution at room temperature (r.t.), are shown in Fig. 2, and the main optical features are summarized in Table 1. All compounds under investigation exhibit an intense absorption band in the visible region, ranging from approximately 485 to 530 nm, with a bathochromic shift in the order **AD418** < **TTZ5** < **BTD-DTP1** (Fig. 2 and Table 1). Based on the push–pull structural design of the dyes and supported by literature data, this band can be confidently attributed to an intramolecular charge transfer (ICT) transition.[31,32,36–39] The intensity of the ICT band increases from 38 600 to 94 100 M^{-1} cm^{-1} in the order **AD418** < **BTD-DTP1** < **TTZ5** (Table 1), reflecting the increasing length of the π–conjugated segment between the donor and the acceptor (D–A) moieties. Conversely, the weaker high-energy bands located in the UV region (*ca.* 300–350 nm) are likely attributable to locally excited (LE) states, mainly involving the π systems of the chromophores.

The emission spectra, obtained in THF at room temperature and in a CH_2Cl_2 : CH_3OH (1 : 1) glassy mixture at 77 K upon excitation at 460 and 455 nm, respectively, are also reported in Fig. 2, with the main photophysical parameters listed in Table 1. The steady-state luminescence spectra exhibit emission maxima between 650 and 670 nm at r.t. The fluorescence quantum yields of **AD418** and **BTD-DTP1** are relatively high (ϕ = 0.45–0.47, Table 1), while **TTZ5** is less emissive, with a lower quantum yield of 0.12 (Table 1). The emission of **AD418** is characterized by a single-exponential decay with a lifetime of 2.5 ns (Table 1), whereas **BTD-DTP1** and **TTZ5** show double-exponential decays. A plausible explanation is the presence of a convoluted dual emission in **BTD-DTP1** and **TTZ5**, arising from two distinct ICT states, a phenomenon previously observed in other push–pull conjugates.[38,40–42] Further investigations were conducted on a CH_2Cl_2 solution of **BTD-DTP1** to test this hypothesis. Both absorption and emission spectra are red-shifted upon changing the solvent from THF to CH_2Cl_2 (Fig. S1). Notably, in CH_2Cl_2, the high-energy absorption shoulder at *ca.* 450 nm disappears and the emission profile broadens. An in-depth analysis has been performed by acquiring excitation–emission maps for **BTD-DTP1** in the two solvents (Fig. S2): the shoulder at 450 nm in the excitation spectrum is evident only in THF, and the emission profile remains unchanged whatever the spanned excitation wavelength. This indicates that the absorption profile in the 400–600 nm region contains the contribution from two different excited states, which are close in energy and spectrally convoluted. Indeed, by applying a Gaussian deconvolution of the absorption profile in both solvents, two components emerge, one at higher and one at lower energy (Fig. S3). Both profiles broaden when moving from THF to CH_2Cl_2 and the one at lower energy undergoes a more pronounced red-shift.

To clarify the nature of the corresponding states, the first 10 excited states of compound **BTD-DTP1** were computed at the

TDDFT level in THF solvent. According to the simulated absorption spectrum shown in Fig. S4 (see also Table S1 for full details on the computed excited states), and in agreement with the Gaussian deconvolution of Fig. S3, there are two absorption maxima in the lowest-energy part of the spectrum, found at 408 and 515 nm, corresponding to excitation energies of 3.04 and 2.41 eV, respectively. The excited state at 2.41 eV corresponds to the excitation of electrons occurring from HOMO to LUMO (74% orbital contribution) and from HOMO−1 to LUMO (15% orbital contribution) transitions. The second excited state at 3.04 eV involves the following orbital contributions: HOMO → LUMO+1 (49%) and HOMO−1 → LUMO (30%). Inspecting the electron density distributions shown in Table S2, it is evident that the HOMOs are mainly localized on the donor and central part of the molecules, with a sizeable contribution from the conjugated carbon scaffolds, while LUMOs feature a significant contribution from the acceptor cyanoacrylic group. The computed electron density distributions indicate the existence of a good degree of intramolecular charge transfer upon photoexcitation.

Table S3 compares the measured emission lifetimes and their fractional intensities in the two solvents, revealing slight differences in their values (from 2.6 to 2.0 ns and from 4.7 to 5.6 ns), along with an increase in the relative intensity of the shorter component when moving from THF to CH_2Cl_2. Moreover, global analysis of the time-resolved spectra indicates that both spectral profiles associated with the two lifetimes undergo a significant red-shift when passing from THF to CH_2Cl_2 (Fig. S5 and S6). These findings support the attribution of the two lifetimes to two different ICT states. These two emissive states thus decay independently and are energetically close in THF, resulting in dual luminescence detectable only through lifetime analysis. The single-exponential decay observed for **AD418** may be due to weak or absent emission from one of the two states.

In the glassy rigid matrix at 77 K, a hypsochromic shift of the emission of the dyes is observed (Fig. 2, dashed blue lines), consistent with the CT nature of the excited states and due to rigidochromic effects that hamper the reorganization of the solvent. While in **AD418** the emission profile is only shifted without significant changes in the spectral shape, for **BTD-DTP1** and **TTZ5** the low temperature also causes an increased asymmetry of the profile. This can be explained by considering that the two above-mentioned transitions have a slightly different ICT character (see Table S2 and previous discussion) and they can be differently affected by the temperature decrease. Excitation spectra, recorded both at RT and at 77 K, show a good match with the absorption features of the dyes (Fig. 2), confirming the genuineness of the emission.

Spectroelectrochemistry. To identify the spectral features of the cationic species of each dye – useful for analyzing fast charge transfer events occurring at the dye/TiO_2 interface (*vide infra*) – a spectroelectrochemical characterization was carried out for the three dyes in CH_2Cl_2 solution. UV-Vis-NIR absorption spectra were recorded under potentiostatic conditions at increasing applied voltages. Cyclic voltammetry data for **AD418**,[31] **BTD-DTP1**,[32] and **TTZ5**,[33,43] in CH_2Cl_2 and $CHCl_3$, reported in the literature, show two oxidation peaks for each compound. Accordingly, spectra were recorded under three conditions: (i) at open-circuit potential (OCP), providing the spectrum of the neutral species; (ii) at a potential between the first and second oxidation peaks, representative of the radical monocationic species; and (iii) at a potential higher than the

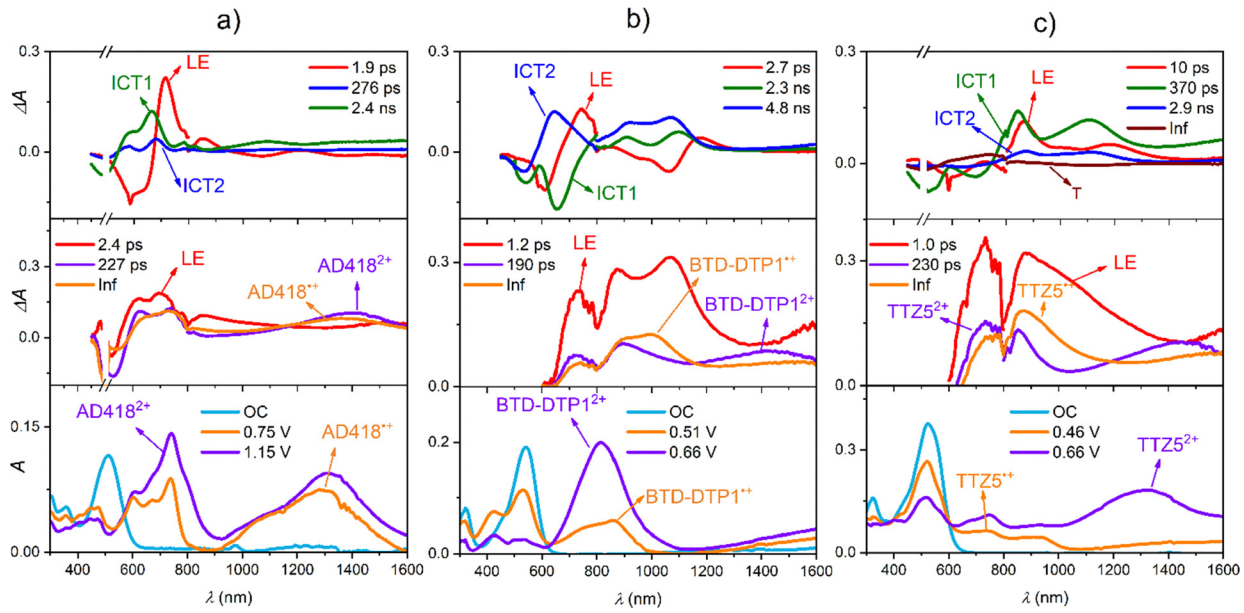

Fig. 3 Comparison among: spectral distributions of pre-exponential amplitudes of calculated lifetimes from global fit analysis performed on TAS (λ_{exc} = 500 nm, E = 3 μJ per pulse) matrices of THF solutions (top) of the dyes (**AD418** (a), **BTD-DTP1** (b) and **TTZ5** (c)), and of electrodes with the dye deposited on a TiO_2 substrate (middle); UV-Vis-NIR absorption spectra (bottom) of the neutral and cationic species of the dyes in $TBAPF_6$ 0.1 M CH_2Cl_2 solution obtained upon application of the specified potentials *vs.* Fc/Fc^+.

second oxidation peak, corresponding to the dicationic species. The collected spectra display two distinct sets of spectral features for each dye, which can thus be attributed to the mono- and di-cationic species (Fig. 3a–c, bottom). The mono-cation of **AD418** exhibits two visible absorption bands of similar intensity at 602 and 737 nm, along with a broad near-infrared band centered at 1295 nm (Fig. 3a, bottom). In contrast, the di-cation shows a more intense band at 740 nm relatively to that at 605 nm. For **BTD-DTP1**, both cationic species display a visible absorption band around 800 nm and an additional band appearing above 1600 nm (Fig. 3b, bottom). The main difference lies in the broader, double-peaked nature of the 800 nm band in the mono-cation, which becomes sharper and more intense in the di-cation. Finally, **TTZ5** shows similar visible bands for both cationic species, whereas in the NIR region, only the di-cation exhibits a pronounced absorption band centered at 1300 nm (Fig. 3c, bottom).

Transient absorption spectroscopy. Femtosecond transient absorption spectroscopy (TAS) has been used to study the excited state deactivation of the dyes, both in THF solution and once anchored on TiO_2 photoelectrodes, in order to characterize photoinduced processes and charge transfer dynamics. Excitation has been performed at 500 nm, since it corresponds to an isosbestic point among the two ICT contributions in the absorption spectrum of the dyes (Fig. S3). The temporal evolution of the TA spectra for the three samples in THF solution (Fig. S7–S9) indicates the presence of different processes. In the end-of-pulse spectra, all the three samples show positive Vis-NIR absorption bands together with a convolution of negative bands with peaks around 500–520 nm and 620–700 nm. Due to the complexity of the transient matrices, a global fit analysis has been applied (the derived spectral distribution of the pre-exponential amplitudes is reported in Fig. 3, top). The spectral profiles of the identified species show some common features among the three dyes: (i) a short-lived species (2–10 ps) displays positive absorption around 700 nm and a stimulated emission band at *ca.* 600 nm (red spectra in the figures); (ii) two other species with longer lifetimes are characterized by ground-state (GS) bleaching features at 500–520 nm, stimulated emission around 650–700 nm and positive bands all-over the spectral range (blue and green spectra). It can be noticed that for **BTD-DTP1** and **TTZ5** the longer lifetimes match those measured with fluorescence analysis (Table 1) and can be thus safely ascribed to the two ICT states previously discussed. The short-lived species can be identified as the LE state that forms upon excitation and then relaxes populating the other two lower lying states. The stimulated emission of this state is indeed blue-shifted with respect to that of the ICT states, detected by steady-state measurements.[44] In the case of **AD418**, together with a species living 2.4 ns, attributed to the emissive ICT state, a second species with a lifetime of 276 ps is detected (Fig. 3a, top). The latter can be ascribed to a relaxed ICT state whose weak emission and/or short lifetime preclude its detection by single photon counting analysis. Eventually, for **TTZ5** a fourth species with an ''infinite'' lifetime (longer than the time scale of the experiment) is observed: it can be attributed to a formed triplet. Indeed, the latter compound displays the lowest fluorescence quantum yield and the highest non-radiative rate constant, suggesting that it could undergo intersystem crossing to the triplet state.

The transient signals of the same dyes deposited on TiO_2 are somehow simpler, with intense positive bands in the Vis-NIR region and a ground-state bleaching band clearly visible only for **AD418** (Fig. S10–S12).[45] No stimulated emission is detected. A global fit analysis has been performed also in this case and the spectral distributions of the pre-exponential amplitudes is reported in Fig. 3, middle. In all cases, three main species are obtained by the fitting: one has a short lifetime of 1–2 ps (red curves), while the other two are associated to lifetimes of *ca.* 200 ps and ''infinite'' (purple and orange curves, respectively). The spectral profile of the short-lived component shows positive bands that resemble those of the excited states detected in solution: both LE and ICT features appear merged in this spectrum, that can be ascribed to a locally excited state populated upon excitation. The packing of the dyes on the TiO_2 surface and the absence of solvent relaxation dynamics in the solid state can explain the observed features. The short lifetime of this state can be attributed to electron injection into TiO_2, allowing to estimate a rate of 1–2 ps for the charge injection process. Similar injection dynamics, in the order of few ps, have been reported for organic dye-sensitized TiO_2 films explored in the absence of an electrolyte.[46–50] Positive bands in the 600–800 nm region of the LE spectrum can mask the presence of stimulated emission. The other two species detected in the solid state might account for cationic forms of the dyes generated upon electron injection. Indeed, the spectra of mono- and di-cationic species collected by spectroelectrochemical experiments (Fig. 3, bottom) present somehow similar features. The differences in the spectral features might arise from the different environment experienced by the dyes on the solid surface with respect to solution. Also, a contribution from the absorption of injected electrons in the IR spectral region of the transient spectra cannot be excluded.[51–55] One of the two species (purple lines in Fig. 3, middle), corresponding to a lifetime in the order of 200 ps, has features more similar to those of the dye's di-cation (particularly evident for **TTZ5**, Fig. 3c), while the other one (orange lines), with an ''infinite'' lifetime, shows a spectral distribution more related to the dye's mono-cation. The presence of di-cationic forms of the dyes can be tentatively ascribed to further processes of oxidation following electron injection. The shorter lifetime of the di-cationic species would testify their higher reactivity and faster recombination rate. We cannot however exclude that both observed species correspond to the dye's radical mono-cation, recombining with electrons in the conduction band with different kinetics. This can be related to different distributions and inhomogeneity of electron–hole pairs in the TiO_2 film.[36,56] Overall, the presence of a long (''infinite'') lifetime for the monocationic species is indicative of the existence of free charges that will give origin to the photocurrent once these photoelectrodes will be employed under working conditions. These proof-of-concept data, obtained in dry films in air, thus

confirm the potential of the three dyes to be employed as photosensitizers in PEC cells.

Experimental

Materials and methods

Spectroscopic grade Uvasol® dichloromethane (CH_2Cl_2) from Merck was treated with dry $CaCO_3$ before use, to eliminate traces of acid. Spectroscopic grade Uvasol® tetrahydrofuran (THF) from Merck was used without further purification. $[Ru(bpy)_3]Cl_2$ was acquired from Carlo Erba and used without further purification.

Synthetic procedures

Dyes **AD418**,[31] **BTD-DTP1**,[32] and **TTZ5**[35] were prepared according to the previously reported synthetic procedures. The corresponding Schemes are shown in the SI (Schemes S1–S3).

Photoelectrodes preparation procedures

10×10 cm^2 FTO-coated conducting glass sheets (TEC 8 Ω sq^{-1}, GreatCell Solar Materials) were cleaned in an ultrasonic bath applying the following consecutive steps: (a) immersion in water with a commercial detergent (15′), and rinsing with demineralized water (3×); (b) immersion in demineralized water (15′), and rinsing with acetone (3×); (c) immersion in acetone (15′). The cleaned sheets were then immersed in boiling *iso*-propanol for a very short time (approx. 10 s) and dried under air.

A single layer of mesoporous TiO_2 was printed on an FTO glass substrate by employing a commercially available nanocrystalline TiO_2 paste (TiO_2 Paste 18NR-T, GreatCell Solar Materials). The paste was mechanically stirred for 20′ prior to use, and then it was printed in 1.0×1.0 cm^2 spots, using an Aurel C920 semi-automatic screen printer. After printing, the plates were put in a chamber filled with EtOH fumes for 30″ to let the paste relax, and were then dried at 120 °C for 30 min. The TiO_2 films were then sintered following a pre-programmed ramp: 15′ at 350 °C, 30′ at 375 °C, 1 h at 450 °C, and 1 h at 500 °C. The active area of the resulting mesoporous semi-transparent TiO_2 films was 1.0 cm^2 and the plates were cut into 2.5×2.5 cm^2 slides. The thickness of the films, measured with a profilometer, was in the order of 5–6 μm.

The sensitization of the films was then carried out by their immersion into 0.1 mM solutions of the dyes in THF for one night, at room temperature. The photoelectrodes were removed from the sensitizing bath, rinsed with THF and dried under air prior to characterization.

Photophysical characterization

Absorption spectra of solutions were recorded with PerkinElmer Lambda 650 UV-Vis or Lambda 950 UV-Vis-NIR spectrophotometers in 1 cm or 2 mm quartz cuvettes. The molar absorption coefficients (ε) were calculated by applying the Lambert–Beer law to low absorbance spectra ($A < 1$) recorded at successive dilutions. Estimated errors are ±1 nm on absorption maxima and <3% for the molar absorption coefficients.

Emission spectra were recorded with an Edinburgh FLS920 spectrofluorometer, equipped with a Peltier-cooled Hamamatsu R928 PMT (280–850 nm). Fluorescence quantum yields (ϕ_{fl}) were evaluated with the comparative method developed by Demas and Crosby,[57] upon correction of the spectra for the wavelength-dependent monochromator/photomultiplier assembly response. As reference, $[Ru(bpy)_3]Cl_2$ in air-equilibrated distilled water (ϕ_{fl} = 0.042)[58] was used. Measurements at 77K were performed using Spectrasil® quartz EPR tubes dipped in liquid nitrogen in a quartz Dewar. Excitation spectra were corrected for the wavelength-dependent lamp intensity. Estimated errors are ±1 nm for the emission maxima and 10% for the quantum yields.

Emission lifetimes in the nanosecond range were determined by using a time-correlated single-photon counting (TCSPC) system consisting of a PicoQuant FluoTime 250 compact lifetime fluorometer, a PicoHarp 330 event timer and TCSPC unit, a PMA 192 detector (230–920 nm) and picosecond pulsed laser diode LEDs (LDH-I series) driven by the Taiko PDL M1 picosecond pulsed driver. The analysis of luminescence decay profiles against time was accomplished using the EasyTau 2 data analysis software (PicoQuant). The estimated error on luminescence lifetimes is 10%. Decay associated spectra (DAS) were obtained by global analysis of the kinetic data by using the global fitting module of the EasyTau 2 software. The wavelength dependences of the amplitudes of the individual kinetic components were plotted as decay associated spectra.

Pump–probe transient absorption measurements were performed in transmission mode for both solutions and solid-state samples with an Ultrafast Systems HELIOS (HE-VIS-NIR) femtosecond transient absorption spectrometer by using, as excitation source, a Newport Spectra Physics Solstice-F-1K-230 V laser system, combined with a TOPAS Prime (TPR-TOPAS-F) optical parametric amplifier (pulse width: 100 fs, 1 kHz repetition rate) tuned at 500 nm. Two sapphire crystals for continuum generation in the visible range (450–800 nm) and in the NIR (800–1600 nm) have been employed. The overall time resolution of the system is 300 fs. Air-equilibrated solutions in 0.2 cm optical path cells were analyzed under continuous stirring. Measurements on the electrodes were carried out in air by placing the electrodes in the sample holder and directing the pump and probe onto the dye-sensitized surface. Monomolecular layers of the organic compound (thickness in the order of a few nm) distributed on the mesoporous TiO_2 surface (thickness in the order of 5–6 μm), can be considered responsible for light absorption. Careful alignment allowed the maximization of pump and probe overlap on the film surface. The pump energy on the sample was 3 μJ per pulse. The diameter of the pump beam is *ca.* 1 mm, while that of the probe beam is *ca.* 0.5 mm. Surface Xplorer V4 software from Ultrafast Systems was used for data acquisition and analysis. The 3D data surfaces were corrected for the chirp of the probe pulse prior to analysis. Global analysis has been performed with the same software on the data surfaces, by fixing principal components *via* single value decomposition and by deriving the spectral distributions of the pre-exponential coefficients of the calculated lifetimes.

Spectroelectrochemical characterization

Spectroelectrochemical measurements were performed on $3 \div 4 \times 10^{-5}$ M CH_2Cl_2 solutions of the dyes. The *in situ* UV-Vis-NIR spectroelectrochemical measurements were carried out with a Metrohm Autolab PGSTAT204 or PGSTAT302N potentiostat/galvanostat and a PerkinElmer Lambda 950 spectrophotometer in a thin layer quartz spectroelectrochemical cell (ALS, model SEC-C). A platinum gauze was used as the working electrode, a platinum wire was the counter electrode, while the reference electrode was made by Ag/Ag^+ ($AgNO_3$ 0.01 M) in acetonitrile (ALS, model RE-7). Tetrabutylammonium hexafluophosphate ($TBAPF_6$) 0.1 M in CH_2Cl_2 was used as the electrolyte. The spectroelectrochemical tests were carried out at room temperature.

Computational details

The absorption maxima (λ_{max}[a]), vertical excitation energies (E_{exc}) and oscillator strengths (f) in THF solution were calculated on the minimum structure of **BTD-DTP1** previously reported,[31] *via* time-dependent DFT (TD-DFT) at the CAM-B3LYP[59]/6-311G(d,p) level of theory, using the Gaussian 16, Revision C.01 suite of programs.[60] Solvent effects have been included by using the polarizable continuum model (PCM).[61]

Conclusions

Absorption and emission spectroscopy of the dyes **AD418**, **BTD-DTP1**, and **TTZ5** reveals that their photophysical behaviour is governed by intramolecular charge transfer (ICT) transitions. Emission studies indicate that **AD418** emits from a single ICT state, with a high fluorescence quantum yield and mono-exponential decay. In contrast, **BTD-DTP1** and **TTZ5** display dual-emission behaviour, originating from two different ICT states. Low-temperature measurements further support the presence of distinct emissive states. Overall, the results demonstrate that both dye structure and environmental factors significantly influence the balance between the two ICT emissions – an essential aspect for optimizing their photophysical performance in applications such as solar energy conversion.

Femtosecond transient absorption spectroscopy (TAS) reveals distinct excited-state dynamics for the three dyes, both in THF solution and when anchored on TiO_2 photoelectrodes. In solution, all dyes exhibit a short-lived LE state that relaxes into longer-lived ICT states. On TiO_2, rapid (1–2 ps) electron injection occurs from a locally excited state, followed by the formation of cationic dye species. Long (''infinite'') lifetimes are observed, indicating efficient charge separation and the potential for sustained photocurrent generation.

Author contributions

F. R.: investigation, data curation, formal analysis, writing – original draft, writing – review & editing; M. B.: investigation, writing – original draft; E. E.: investigation, writing – original draft; E. B.: investigation, writing – review & editing; A. B.: funding acquisition, writing – original draft, writing – review & editing; A. S.: computational calculations, data curation, writing – original draft, writing – review & editing; A. M.: funding acquisition, conceptualization, supervision, writing – review & editing; L. Z.: funding acquisition, conceptualization, supervision, writing – original draft, writing – review & editing; B. V.: investigation, supervision, writing – original draft, writing – review & editing.

Conflicts of interest

There are no conflicts to declare.

Data availability

The data supporting this article have been included as part of the supplementary information (SI). Supplementary information: synthetic procedures, absorption, emission and decay associated spectra, computational data, pump-and-probe transient absorption spectra. See DOI: https://doi.org/10.1039/d6cp00604c.

Acknowledgements

The authors thank the European Union – NextGeneration EU, PNRR M2C2, Investment 3.5, POR H2 AdP MMES/ENEA-CNR-RSE, project ''Research and development of technologies for the hydrogen supply chain'' – CUP B93C22000630006, for financial support. AS thanks the Ministero dell'Ambiente e della Sicurezza Energetica (SOLE-H2, Project RSH2A_000004 – CUP F57G25000080006, funded by European Union—NextGenerationEU, Piano Nazionale di Ripresa e Resilienza (PNRR) Missione 2 Componente 2 Investimento 3.5—D.D. 279 05/08/2025).

Notes and references

1 Y. Liu, S. Bai, F. Wang and Y. Chen, *Environ. Chem. Lett.*, 2021, **20**, 1169–1192.
2 L. Clarizia, M. N. Nadagouda and D. D. Dionysiou, *Curr. Opin. Green Sustain. Chem.*, 2023, **41**, 100825.
3 B. Liu, S. Wang, G. Zhang, Z. Gong, B. Wu, T. Wang and J. Gong, *Chem. Soc. Rev.*, 2023, **52**, 4644–4671.
4 L. Zani, M. Melchionna, T. Montini and P. Fornasiero, *J. Phys. Energy*, 2021, **3**, 031001.
5 S. Zhang, H. Ye, J. Hua and H. Tian, *EnergyChem*, 2019, **1**, 100015.
6 M. K. Brennaman, R. J. Dillon, L. Alibabaei, M. K. Gish, C. J. Dares, D. L. Ashford, R. L. House, G. J. Meyer, J. M. Papanikolas and T. J. Meyer, *J. Am. Chem. Soc.*, 2016, **138**, 13085–13102.
7 B. Zhang and L. Sun, *Chem. Soc. Rev.*, 2019, **48**, 2216–2264.
8 M. Z. Qamar, F. K. Asiam, H. C. Kang, R. Shahid, A. K. Kaliamurthy, C. Chen, J. Lim, M. M. Rahman and J. J. Lee, *Small*, 2025, **21**, e2411853.

9 X.-L. Wang, J.-F. Huang, J.-M. Liu and P. Tsiakaras, *Coord. Chem. Rev.*, 2025, **522**, 216143.
10 F. Bureš, *RSC Adv.*, 2014, **4**, 58826–58851.
11 C. Decavoli, C. L. Boldrini, N. Manfredi and A. Abbotto, *Eur. J. Inorg. Chem.*, 2020, 978–999.
12 S. Kato and F. Diederich, *Chem. Commun.*, 2010, **46**, 1994–2006.
13 H. Ye, L. Shen, S. Zhang, X. Li, F. Yu, R. Diao and J. Hua, *ACS Omega*, 2018, **3**, 14448–14456.
14 M. A. M. Rashid, D. Hayati, K. Kwak and J. Hong, *Nanomaterials*, 2019, **9**, 119.
15 F. A. Black, C. A. Clark, G. H. Summers, I. P. Clark, M. Towrie, T. Penfold, M. W. George and E. A. Gibson, *Phys. Chem. Chem. Phys.*, 2017, **19**, 7877–7885.
16 N. Manfredi, C. L. Boldrini and A. Abbotto, *ChemElectroChem*, 2018, **5**, 2395–2402.
17 M. S. Eberhart, D. Wang, R. N. Sampaio, S. L. Marquard, B. Shan, M. K. Brennaman, G. J. Meyer, C. Dares and T. J. Meyer, *J. Am. Chem. Soc.*, 2017, **139**, 16248–16255.
18 M. Yamamoto, Y. Nishizawa, P. Chabera, F. Li, T. Pascher, V. Sundstrom, L. Sun and H. Imahori, *Chem. Commun.*, 2016, **52**, 13702–13705.
19 D. Antón-García, E. Edwardes Moore, M. A. Bajada, A. Eisenschmidt, A. R. Oliveira, I. A. C. Pereira, J. Warnan and E. Reisner, *Nat. Synth.*, 2022, **1**, 77–86.
20 L. Nhon, B. Shan, A. D. Taggart, R. M. W. Wolfe, T. T. Li, C. M. Klug, A. Nayak, R. M. Bullock, J. F. Cahoon, T. J. Meyer, K. S. Schanze and J. R. Reynolds, *ACS Appl. Mater. Interfaces*, 2021, **13**, 47499–47510.
21 T. Luo, X.-A. Li, C.-J. Bai, C.-Y. Lv, J.-F. Huang and J.-M. Liu, *ACS Appl. Energy Mater.*, 2021, **4**, 14671–14680.
22 K. Tang, J. Y. Shao and Y. W. Zhong, *Chem. Commun.*, 2023, **59**, 6072–6075.
23 L. Alibabaei, R. J. Dillon, C. E. Reilly, M. K. Brennaman, K. R. Wee, S. L. Marquard, J. M. Papanikolas and T. J. Meyer, *ACS Appl. Mater. Interfaces*, 2017, **9**, 39018–39026.
24 T. Luo, J. Huang and J. Liu, *Chem. Res. Chin. Univ.*, 2020, **36**, 1091–1096.
25 J. H. Yum, T. W. Holcombe, Y. Kim, K. Rakstys, T. Moehl, J. Teuscher, J. H. Delcamp, M. K. Nazeeruddin and M. Gratzel, *Sci. Rep.*, 2013, **3**, 2446.
26 L. Yu, J. Xi, H. T. Chan, T. Su, L. J. Antrobus, B. Tong, Y. Dong, W. K. Chan and D. L. Phillips, *J. Phys. Chem. C*, 2013, **117**, 2041–2052.
27 H. Tian, I. Bora, X. Jiang, E. Gabrielsson, K. M. Karlsson, A. Hagfeldt and L. Sun, *J. Mater. Chem.*, 2011, **21**, 12462–12472.
28 R. Misra and S. P. Bhattacharyya, *Intramolecular Charge Transfer: Theory and Applications*, Wiley-VCH Verlag, Weinheim, Germany, 2018.
29 W. J. Youngblood, S. H. Lee, K. Maeda and T. E. Mallouk, *Acc. Chem. Res.*, 2009, **42**, 1966–1973.
30 D. A. Wheeler, G. Wang, Y. Ling, Y. Li and J. Z. Zhang, *Energy Environ. Sci.*, 2012, **5**, 6682–6702.
31 A. Dessì, M. Monai, M. Bessi, T. Montini, M. Calamante, A. Mordini, G. Reginato, C. Trono, P. Fornasiero and L. Zani, *ChemSusChem*, 2018, **11**, 793–805.
32 A. Dessì, D. A. Chalkias, S. Bilancia, A. Sinicropi, M. Calamante, A. Mordini, A. Karavioti, E. Stathatos, L. Zani and G. Reginato, *Sustain. Energy Fuels*, 2021, **5**, 1171–1183.
33 A. Dessì, M. Calamante, A. Mordini, M. Peruzzini, A. Sinicropi, R. Basosi, F. Fabrizi de Biani, M. Taddei, D. Colonna, A. Di Carlo, G. Reginato and L. Zani, *Chem. Commun.*, 2014, **50**, 13952–13955.
34 L. Vesce, P. Mariani, M. Calamante, A. Dessì, A. Mordini, L. Zani and A. Di Carlo, *Sol. RRL*, 2022, **6**, 2200403.
35 M. L. Parisi, A. Dessì, L. Zani, S. Maranghi, S. Mohammadpourasl, M. Calamante, A. Mordini, R. Basosi, G. Reginato and A. Sinicropi, *Front. Chem.*, 2020, **8**, 214.
36 X. Yzeiri, N. Sangiorgi, F. Gambassi, A. Barbieri, M. Calamante, D. Franchi, C. Coppola, A. Sinicropi, B. Ventura, A. Mordini, A. Sanson and L. Zani, *Dyes Pigm.*, 2025, **232**, 112455.
37 C. Papucci, A. Dessì, C. Coppola, A. Sinicropi, G. Santi, M. Di Donato, M. Taddei, P. Foggi, L. Zani, G. Reginato, A. Pucci, M. Calamante and A. Mordini, *Dyes Pigm.*, 2021, **188**, 109207.
38 N. A. Sayresmith, A. Saminathan, J. K. Sailer, S. M. Patberg, K. Sandor, Y. Krishnan and M. G. Walter, *J. Am. Chem. Soc.*, 2019, **141**, 18780–18790.
39 M. Bartolini, V. Gombac, A. Sinicropi, G. Reginato, A. Dessì, A. Mordini, J. Filippi, T. Montini, M. Calamante, P. Fornasiero and L. Zani, *ACS Appl. Energy Mater.*, 2020, **3**, 8912–8928.
40 B. Carlotti, A. Cesaretti, C. G. Fortuna, A. Spalletti and F. Elisei, *Phys. Chem. Chem. Phys.*, 2015, **17**, 1877–1882.
41 H. Mandal, J. L. Rao, J. Kulhánek, F. Bureš and P. R. Bangal, *J. Phys. Chem. C*, 2023, **127**, 4724–4740.
42 Z. R. Grabowski, K. Rotkiewicz and W. Rettig, *Chem. Rev.*, 2003, **103**, 3899–4032.
43 A. Dessì, M. Calamante, A. Mordini, M. Peruzzini, A. Sinicropi, R. Basosi, F. Fabrizi de Biani, M. Taddei, D. Colonna, A. di Carlo, G. Reginato and L. Zani, *RSC Adv.*, 2015, **5**, 32657–32668.
44 J. Cerezo, S. Gao, N. Armaroli, F. Ingrosso, G. Prampolini, F. Santoro, B. Ventura and M. Pastore, *Molecules*, 2023, **28**, 3910.
45 For **BTD-DTP1** and **TTZ5** the strong GS absorption precludes the detection of the signals below 620 nm.
46 M. Fakis, M. Dori, E. Stathatos, H.-H. Chou, Y.-S. Yen, J. T. Lin, V. Giannetas and P. Persephonis, *J. Photochem. Photobiol., A*, 2013, **251**, 18–24.
47 M. Giannouli and M. Fakis, *J. Photochem. Photobiol., A*, 2011, **226**, 42–50.
48 D. M. Niedzwiedzki, D. Unny, G. R. Kandregula and K. Ramanujam, *Dyes Pigm.*, 2022, **202**, 110273.
49 C. Martín, M. Ziółek and A. Douhal, *J. Photochem. Photobiol., C*, 2016, **26**, 1–30.
50 J. Sobuś, J. Karolczak, D. Komar, J. A. Anta and M. Ziółek, *Dyes Pigm.*, 2015, **113**, 692–701.
51 F. M. Pesci, A. J. Cowan, B. D. Alexander, J. R. Durrant and D. R. Klug, *J. Phys. Chem. Lett.*, 2011, **2**, 1900–1903.

52 S. Corby, L. Francas, S. Selim, M. Sachs, C. Blackman, A. Kafizas and J. R. Durrant, *J. Am. Chem. Soc.*, 2018, **140**, 16168–16177.
53 P. Vecchi, F. Ruani, M. Mazzanti, Q. R. Loague, R. Mazzaro, F. Boscherini, B. Ventura, G. J. Meyer, N. Armaroli, S. Caramori and L. Pasquini, *ACS Energy Lett.*, 2024, **9**, 2193–2200.
54 X. He, G. Zhu, J. Yang, H. Chang, Q. Meng, H. Zhao, X. Zhou, S. Yue, Z. Wang, J. Shi, L. Gu, D. Yan and Y. Weng, *Sci. Rep.*, 2015, **5**, 17076.
55 A. Yamakata, T.-a. Ishibashi and H. Onishi, *Chem. Phys. Lett.*, 2001, **333**, 271–277.
56 G. Ramakrishna, A. Das and H. N. Ghosh, *Langmuir*, 2004, **20**, 1430–1435.
57 G. A. Crosby and J. N. Demas, *J. Phys. Chem.*, 1971, **75**, 991–1024.
58 M. Montalti, A. Credi, L. Prodi and M. T. Gandolfi, *Handbook of Photochemistry*, CRC Press, Boca Raton, FL, USA, 3rd edn, 2006.
59 T. Yanai, D. P. Tew and N. C. Handy, *Chem. Phys. Lett.*, 2004, **393**, 51–57.
60 M. J. Frisch, G. W. Trucks, H. B. Schlegel, G. E. Scuseria, M. A. Robb, J. R. Cheeseman, G. Scalmani, V. Barone, G. A. Petersson, H. Nakatsuji, X. Li, M. Caricato, A. V. Marenich, J. Bloino, B. G. Janesko, R. Gomperts, B. Mennucci, H. P. Hratchian, J. V. Ortiz, A. F. Izmaylov, J. L. Sonnenberg, Williams, F. Ding, F. Lipparini, F. Egidi, J. Goings, B. Peng, A. Petrone, T. Henderson, D. Ranasinghe, V. G. Zakrzewski, J. Gao, N. Rega, G. Zheng, W. Liang, M. Hada, M. Ehara, K. Toyota, R. Fukuda, J. Hasegawa, M. Ishida, T. Nakajima, Y. Honda, O. Kitao, H. Nakai, T. Vreven, K. Throssell, J. A. Montgomery Jr., J. E. Peralta, F. Ogliaro, M. J. Bearpark, J. J. Heyd, E. N. Brothers, K. N. Kudin, V. N. Staroverov, T. A. Keith, R. Kobayashi, J. Normand, K. Raghavachari, A. P. Rendell, J. C. Burant, S. S. Iyengar, J. Tomasi, M. Cossi, J. M. Millam, M. Klene, C. Adamo, R. Cammi, J. W. Ochterski, R. L. Martin, K. Morokuma, O. Farkas, J. B. Foresman and D. J. Fox, 2016.
61 J. Tomasi, B. Mennucci and R. Cammi, *Chem. Rev.*, 2005, **105**, 2999–3093.